JOURNAL OF SOLID STATE CHEMISTRY 93, 96–118 (1991)

Interaction of Oxygen with Mo(100), Mo(110), and Mo(111) Surfaces. RHEED and AES Analyses of the Molybdenum Oxide Nucleation and Growth

N. FLOQUET AND O. BERTRAND

Université de Bourgogne, Laboratoire de Recherches sur la Réactivité des Solides, URA 23 CNRS, B.P.138, 21004 Dijon Cedex, France

Received October 9, 1990; in revised form March 4, 1991

A study of the nucleation and growth of MoO_3 generated by interaction of oxygen with Mo(100), Mo(110), and Mo(111) single crystalline surfaces is investigated at high oxygen pressure (10^4 Pa) and low temperature (620 to 820 K). The results of RHEED and AES analyses prove that under these oxidation conditions, MoO_3 nucleates directly from the metal without intermediate formation of MoO_2 or nonstoichiometric molybdenum oxide such as Mo_4O_{11}. The structure and orientation of MoO_3 nuclei are characterized in relation with the parent molybdenum surface. On the Mo(110) and Mo(111) surfaces, which are faceting, the nucleation and growth of MoO_3 takes place by successive structural steps. On the Mo(100) surface, epitaxial relations induce the formation of MoO_3(010) plates oriented onto the Mo surface, which stabilizes and makes passive the Mo(100) surface. The features of the nucleation and growth of MoO_3 are interpreted as linked respectively to structural relations of the metal–oxide interface and to preferential diffusion paths of oxygen through MoO_3.

1. Introduction

Molybdenum is an important alloying metal that is utilized in many technologies requiring high temperature. For this reason, numerous investigations relate to the interaction of molybdenum surfaces with oxygen at low pressure and high temperature. They give detailed results about oxygen chemisorption, surface faceting, and the epitaxial formation of MoO_2 crystallites (*1–22*). Some results of a recent work (*16*) establish that for long oxygen exposure, amorphous MoO_3 (presumably disordered) and intermediate oxides are formed, mixed with MoO_2 crystallites on the Mo(112) faces created on a Mo(111) surface. Other investigations do not relate more, about MoO_3 or intermediate oxide formation, because the MoO_3 phase is highly volatile under these particular oxidation conditions.

Molybendum oxide is an excellent catalyst for the partial oxidation of olefins and alcohols and the reduction of nitric oxide. Earlier thermodynamic studies (*23–34*) and our recent works (*35–36*) on the oxidation of molybdenum foils investigated in a temperature range from 733 to 953 K and under high oxygen pressure (2.7×10^3 and 8×10^4 Pa) prove that the oxidation of molybdenum foils leads to MoO_3 scales, with a preferential orientation of the crystallites.

In view of these previous data, the purpose of the present investigation is double. The fundamental aim is to characterize the mechanisms of nucleation and growth of

0022-4596/91 $3.00

MoO_3 produced by the interaction of oxygen with a molybdenum single crystal surface. The applied aim is to control the elaboration of the MoO_3 crystals for catalytic applications, considering that the catalytic properties of MoO_3 are known to be sensitive to the superficial structures of the exposed faces of MoO_3 crystals.

We have explored oxide formation starting with the clean Mo(100), Mo(110), Mo(111) crystal faces of molybdenum in the temperature range of 620 to 820 K and in the oxygen pressure range of 2.7×10^3 and 4×10^4 Pa.

The changing surface structures were monitored by reflection high-energy electron diffraction (RHEED) and the variations of surface composition and metal oxidation states were measured by Auger electron spectroscopy (AES) peak ratios and peak shapes.

2. Experimental

2.1 Apparatus

Preparation and oxidation experiments were run in a high pressure reaction chamber equipped, among the usual equipment, with an argon ion gun and an infrared reflector heating samples at its focalization point up to 1723 K in vacuum. The sample temperature was monitored by use of a Pt–Pt (10% Rh) thermocouple which was mechanically affixed to the crystal. Research-grade argon and oxygen were admitted into the reaction chamber through variable leak valves. Low and high pressures were taken from the readings of an ion gauge and a Bourdon gauge, respectively.

Chemical and structural analyses were carried out in a standard UHV chamber with CMA-AES and RHEED equipment. The two chambers are connected through a vacuum interlock. The samples were transferred from each to other by means of a magnetic transfer system. They were placed in a high-precision manipulator which controls accurately the angular (to 1 degree) and azimuthal (to 1/10 degree) orientation of the sample with respect to the AES and RHEED analyzers.

The CMA with a colinear electron gun operated either at 1.5 or 2.5 KeV to prevent sample damage was used for the Auger measurements. A 4-V peak-to-peak modulation amplitude was used for most measurements and gave good sensitivity without appreciable distortion of the peak shapes. Some data were collected using a 1-V peak-to-peak modulation amplitude to distinguish changes in the carbon and molybdenum peak shape.

The RHEED gun was operated at 40 kV and the electron beam was directed onto the crystal surface at a glancing angle between 5° and 1°. The sample manipulator allowed RHEED observations along a 120° azimuth of the crystal.

2.2 Preparation and Cleaning of Molybdenum Surfaces

Electron beam-melted single crystals were grown by the floating zone technique from molybdenum bars, 5 mm in diameter, by T. N. Nowicki (*37*). The crystals were oriented to ±1° of the Mo(*hkl*) planes by the Läue X-ray diffraction technique and were cut using a metal-bonded diamand saw. After being cut, the samples were mechanically polished with diamand paste and finally electropolished in an ethanol, methanol, sulfuric acid solution.

Following introduction into the reaction chamber, the sample was initially treated by extensive heating in oxygen at a pressure of 1.3×10^{-5} Pa and temperatures up to 1000 K to reduce bulk carbon. Repeated argon ion bombardments readily removed oxygen and sulfur, but induced bulk carbon segregation. Fine structure on the low energy side of the C(272) Auger transition proved the carbidic nature of the overlayer. Subsequent annealing at 1200 K gave rise to Mo_2C layers epitaxied on the Mo surface as characterized by RHEED patterns and AES data (see Section 3.3.1). Heating to 1000 K for

several minutes in oxygen at pressure of 1.3 $\times$ 10^{-5} Pa removed the Mo_2C overlayers. These cleaning procedures were repeated until AES indicated less than 0.1 monolayer of oxygen and RHEED patterns characterized a well-ordered surface.

The AES and RHEED patterns from a Mo(110) surface following these stages of cleaning are shown in Fig. 1.

2.3 Oxidation Experiments

Experimental oxidation conditions are closely linked to the thermodynamic data for the molybdenum oxygen system (*38–41*). Schematically, under about 10^4 Pa oxygen pressure (*31–32*), from 673 K molybdenum undergoes oxidation into molybdenum oxide solids. No volatile oxides are formed. From 773 K, the sublimation of MoO_3 solid is beginning. The most prominent species are the MoO_3 trimerics (*42–43*). From 1073 K, the liquefaction of MoO_3 solid is arising.

In the explored temperature range choosen between 620 and 820 K and the oxygen pressure range at about 2.7 $\times$ 10^3 Pa, the phenomena of both molybdenum oxide solid formation and MoO_3 sublimation will occur.

The exposures of the Mo(100), Mo(110), and Mo(111) surfaces to oxygen were run in the reaction chamber with the following procedure: oxygen gas was first introduced at 2.7 $\times$ 10^3 Pa pressure, then the crystal surface was heated by means of the calibrated infrared reflector. The exposure time over, heating was stopped and gas was rapidly evacuated. The sample was then transferred in the UHV chamber for AES and RHEED analyses, successively.

3. Results and Discussions

RHEED and AES analyses of the oxidized surface are realized after each exposure lasting between several minutes and a few hours.

Molybdenum Oxides Structural Data

RHEED patterns are interpreted, comparing them with theoretical or experimental diffraction patterns obtained from known structures of the different molybdenum oxides or from natural faces of our synthetized crystals such as MoO_3, $Mo_{18}O_{52}$, Mo_9O_{26}, Mo_8O_{23}, Mo_4O_{11}, MoO_2 (*44–47*).

MoO_3 has an orthorhombic structure (a = 3.96 Å, b = 13.86 Å, c = 3.69 Å) formed by the stacking of two-level MoO_6 layers parallel to MoO_3(010). The relative displacements of the double layers are so connected that the outside oxygen atoms in one layer are placed between the outside oxygen atoms of the neighboring layers (Fig. 2). Successive layers parallel to the MoO_3(010) planes are linked together by Van der Waals interactions. In such a structure, MoO_6 octahedra are relatively distorted (*48*).

The MoO_2 structure built with MoO_6 octahedra is generally described as monoclinic (deformed rutile type) with the parameters a = 5.61 Å, b = 4.85 Å, c = 5.63 Å, β = 120°57. Along MoO_2[100], the MoO_6 octahedra are joined by sharing edges to form strings (Fig. 3) (*49, 50*). The structure is very nearly hexagonal with an a/c ratio of 1.16. The monoclinic–hexagonal translation is made by assuming β = 120° and a = c.

The structure of the nonstoichiometric oxides can be described as built up of MoO_6 octahedra and MoO_4 tetrahedra, more or less distorted (*51, 52*). The $Mo_{18}O_{52}$ oxide is built up of MoO_3 orthorhombic slabs of finite width joined by crystallographic shear planes (CS planes) of MoO_4 tetrahedra. Mo_9O_{26}, Mo_8O_{23}, Mo_4O_{11} are formed of MoO_3 cubic (ReO_3 type) slabs of finite width, joined by CS planes of MoO_4 tetrahedra. Table I gives the crystallographic data of these oxides.

Molybdenum Oxide Auger Spectra

In the same manner, Auger spectra are systematically compared with standard spectra obtained either from natural faces

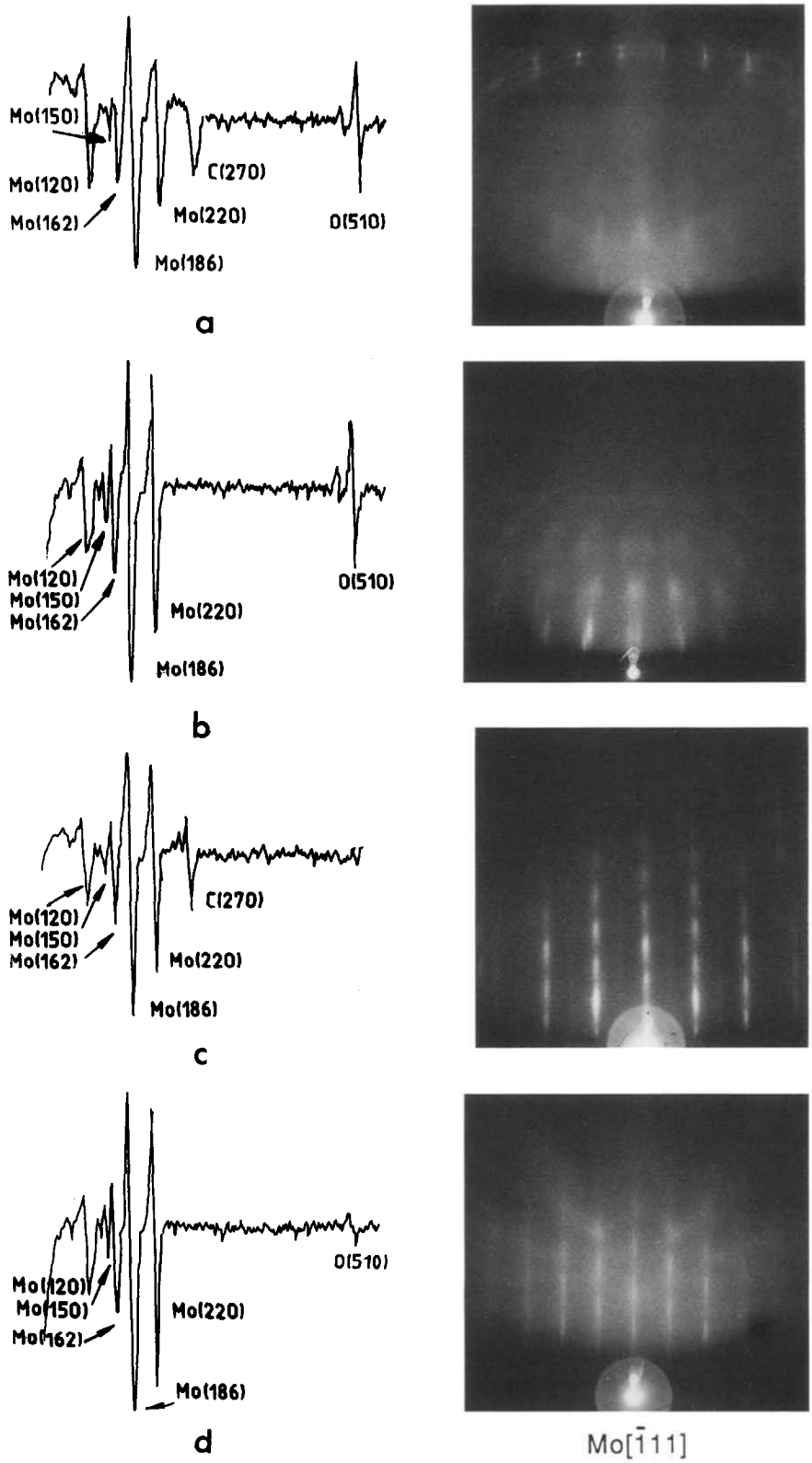

FIG. 1. AES and RHEED patterns from a Mo(110) surface at the various stages of cleaning: (a) electropolished, (b) heated 2 hr in 1.3×10^{-5} Pa oxygen at 1000 K, (c) ions argon bombarded for 10 min at 300 K, (d) cleaned and structured.

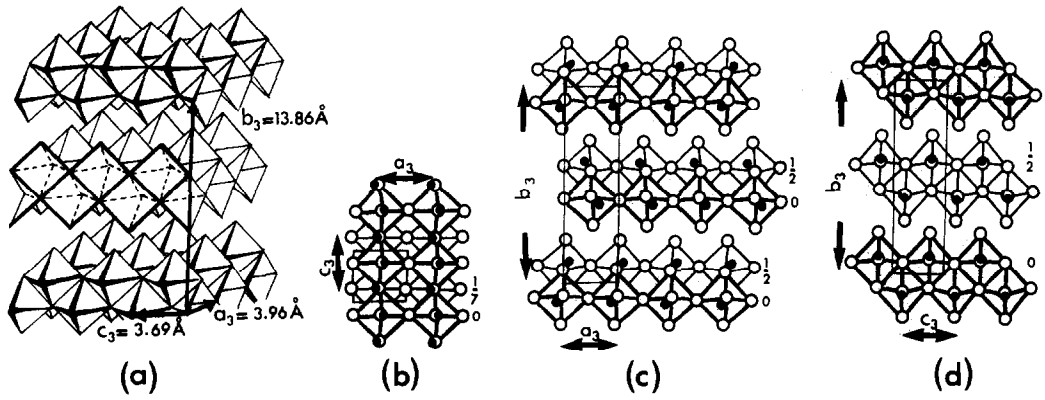

FIG. 2. (a) MoO_3 orthorhombic structure formed by two levels of MoO_6 octahedra layers linked by Van der Waals interactions, (b) [010], (c) [001], (d) [100] projections of MoO_3 structure (a = 3.96 Å, b = 13.86 Å, c = 3.69 Å).

of single crystals such as $MoO_3(010)$ and $MoO_2(001)$ faces, or from a thick film of MoO_3 and MoO_2 crystallites produced by controlled oxidation of a molybdenum sheet.

According to the results reported by Lin and Lichtmann (*53*) and S. Yashonath *et al.* (*54*), the distinctions between the standard spectra of the Mo, MoO_2, and MoO_3 surfaces are relatively small, though detectable and reproducible.

In first derivation spectra, the energy and the lineshape of the molybdenum $M_{4,5}VV$ and $M_{4,5}N_{2,3}V$ Auger transitions change as reported in Fig. 4. The ratios of the peak-to-peak height of these same molybdenum Auger transitions vary systematically with the number of valence electrons or the oxidation number, Z, of the metal, as shown in

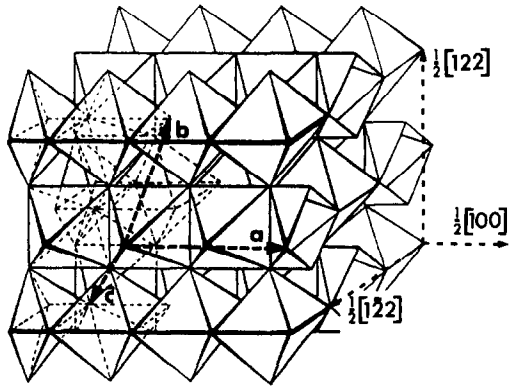

FIG. 3. MoO_2 structure. Described in the monoclinic system (a = 5.61 Å, b = 4.85 Å, c = 5.63 Å, β = 120°57), it is too nearly hexagonal ($a \cong c$, $\beta \cong 120°$). It too could be described as tetragonal by building the elementary cell from 1/2[122] = 6.86 Å, 1/2[1$\bar{2}$2] = 6.86 Å, and 1/2[100] = 2.80 Å.

TABLE I

	Systems	Parameters
$Mo_{18}O_{52}$ $MoO_{2.888}$	Triclinic	a = 8.145 Å α = 95.47° b = 11.89 Å β = 90.39° c = 19.66 Å γ = 109.97°
Mo_9O_{26} $MoO_{2.888}$	Monoclinic	a = 16.74 Å b = 4.019 Å β = 95.45° c = 14.53 Å
Mo_8O_{23} $MoO_{2.875}$	Monoclinic	a = 16.90 Å b = 4.019 Å β = 106.27° c = 14.53 Å
Mo_4O_{11} $MoO_{2.75}$	Orthorhombic	a = 24.40 Å b = 5.450 Å c = 6.723 Å

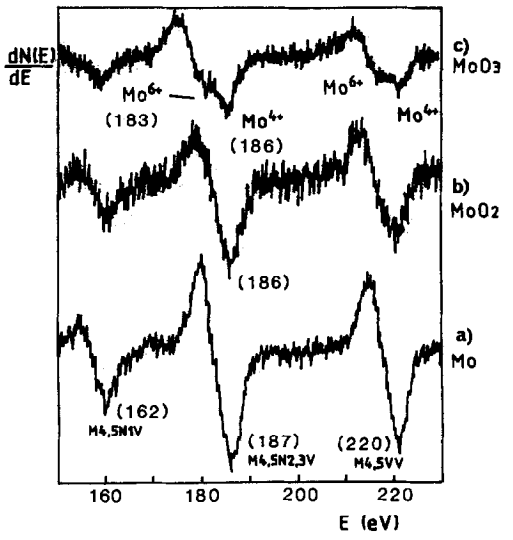

FIG. 4. Mo Auger MNN valence spectra of (a) Mo(110) surface, (b) MoO_2(001) surface, (c) nonstoichiometric MoO_3(010) surface. Beam energy Ep = 2500 eV, modulation voltage = 1 V peak-to-peak.

Fig. 5. Lastly, the oxygen $KL_{2,3}L_{2,3}$ transition intensity referred to the molybdenum $M_{4,5}VV$ transition intensity is, respectively, 3 ± 0.2 for MoO_2 and 4.1 ± 0.2 for MoO_3.

The features of the standard spectra show that the simultaneous formation of MoO_2 and MoO_3 phases should be more evidenced by the values of the ratios of the molybdenum Auger transitions.

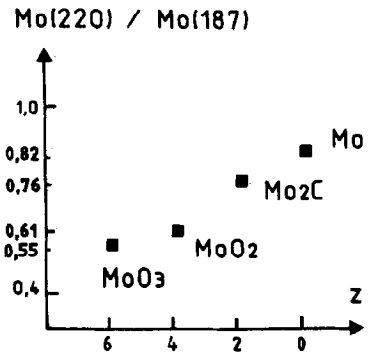

FIG. 5. Dependence of Auger intensity ratios ($R = I_{M4,5VV}/I_{M4,5N2,3V}$) of molybdenum and its oxides on the oxidation number Z.

3.1 Oxidation on the Mo(110) Surface

3.1.1 Temperature of 620 K

At oxygen pressure of 2.7×10^3 Pa, RHEED patterns of the smooth Mo(110) surface (Fig. 6a) fade in a diffuse intensity background and modifications in the Auger spectra characterize the MoO_2 presence: the peak height ratio Mo(220)/Mo(187) decreases from 0.85 to 0.62 and the ratio O(510)/Mo(220) increases from 0.1 to 2.9. There is no $M_{4,5}VV$ splitting, no new peak lower than the $M_{4,5}N_{2,3}V$ transition. The presence of the C(272) peak indicates the carbon adsorption in the graphite form.

After a few minutes exposure, no noticeable changes occur in the Auger spectra, but new RHEED patterns (Fig. 6b) appear: reflection spots are large and elongated perpendicular to the crystal surface, resulting from flat MoO_2 crystallites, in epitaxial relation with the Mo(110) surface:

$$MoO_2(010)_{[100]} \parallel Mo(110)_{[1\bar{1}1]} \text{ or}_{[11\bar{1}]}.$$

Similar expitaxied MoO_2 crystallites were reported by Kennet (*12*) for exposure of 3×10^{-2} Pa · sec oxygen at 900 K and by Brückner (*10*) for 1.3×10^{-5} and 1.3×10^{-1} Pa · sec oxygen exposure at 1000 K onto the Mo(110) surface.

The Auger spectra and the new RHEED patterns are stable under any further oxygen exposure. Exposures at 4×10^{-4} Pa oxygen and higher temperature (820 K) result in the same Auger spectra and more diffuse RHEED patterns. These results show that MoO_3 is not formed; the overlayers of MoO_2 crystallites seem to impede the molybdenum oxidation.

3.1.2. Temperature of 720 K

At the first oxygen exposure, the Auger spectra change markedly, which character-

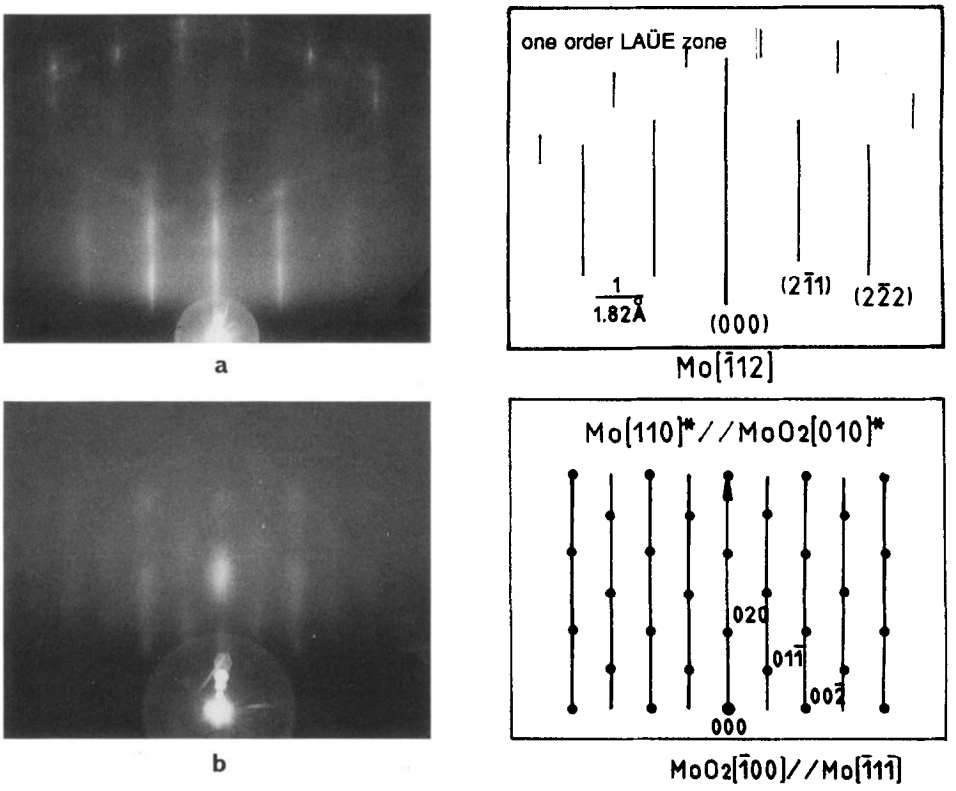

FIG. 6. RHEED patterns from a Mo(110) surface oxidized at 620 K and 2.7 × 10^4 Pa oxygen pressure for increasing exposure time: (a) initial Mo(110) surface, (b) after 5 min.

ize the MoO_3 formation: $M_{4,5}VV$ peak splitting, a new peak at 183 eV lower than the $M_{4,5}N_{2,3}V$ peak by about 4 eV. The peak height ratio Mo(220)/Mo(187) decreases to 0.56 and the ratio O(510)/Mo(220) increases to 4.1. For further exposures no noticeable changes occur in these Auger spectra.

RHEED patterns (Fig. 7) evidence the formation of MoO_3 crystallites on the Mo(110) surface by successive structural steps.

At the first exposure, streak patterns of the Mo(110) surface disappear for a set of thin rings of uniform intensity, at any azimuth (Fig. 7a). This set of rings corresponds to the (100), (110), (210), and (230) rings of the orthorhombic MoO_3 structure. It does not correspond to the strong rings of the MoO_3 structure that are (021), (110), and (040) rings. It is interpreted as the formation of MoO_3[100] whiskers in random orientation on the Mo(110) surface.

After a 1-hr exposure, RHEED patterns change and become differentiated for a specific azimuth of the initial Mo(110) surface (Fig. 7b): previous MoO_3 rings become modulated in intensity and less or more diffuse arcs of new MoO_3 rings appears. The maxima of intensity are arranged in three networks of parallel lines which have the same MoO_3[100] periodicity (4 Å) and are parallel to the Mo(100), Mo(101), and Mo(112) faces of the Mo crystal. These diffraction patterns are interpreted by the growth of MoO_3[100] rods perpendicularly to each Mo(100), Mo(101), and Mo(112) facet simultaneously

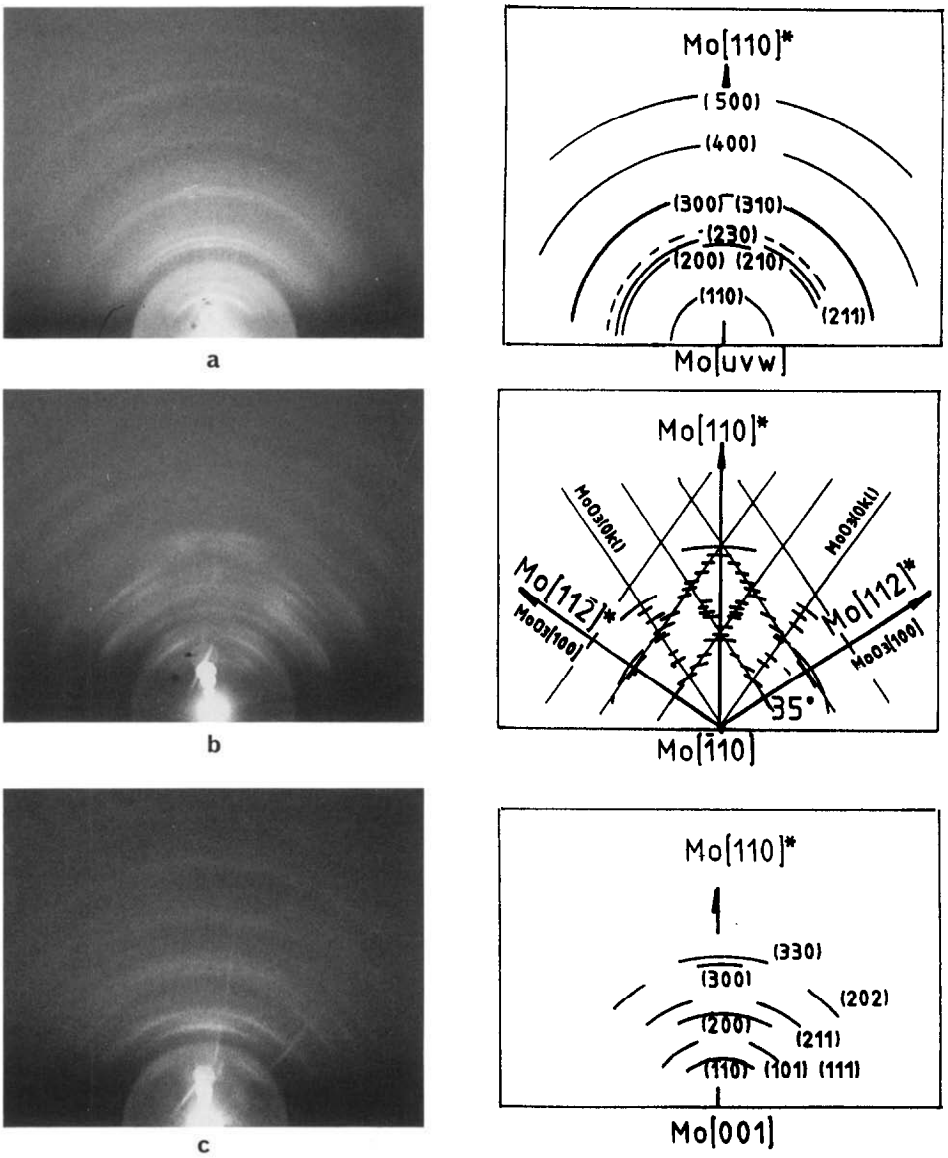

FIG. 7. RHEED patterns from a Mo(110) surface oxidized at 720 K and 2.7×10^4 Pa oxygen pressure for increasing exposure time: (a) after 5 min, (b) after 1 h, (c) after several hours.

formed onto the Mo(110) surface during the oxidation process.

Further exposures, until 8 hr and more, result in a final modification of the RHEED patterns. The maxima of intensity of the MoO_3 rings are arranged on a set of lines with MoO_3[100] periodicity and parallel to the Mo(110) surface. The patterns in the Mo[001] and Mo[1$\bar{1}$0] azimuths are distinguished (Fig. 7c). These last diffraction features characterize MoO_3 rods whose elongated MoO_3[100] axes grow perpendicular

to the initial Mo(110) surface and MoO_3[001] rows are parallel to the Mo[110] direction of the molybdenum surface:

$$MoO_3(100)_{[001]} \parallel Mo(110)_{[1\bar{1}0]}.$$

Compared with RHEED patterns of MoO_3 single crystals, all these observed patterns reveal that the structure of the grown MoO_3 crystallites is never well organized. Accurate analyses specify their structural evolution: first MoO_3[100] rows, oriented perpendicular to the molybdenum facets, are short range ordered in the perpendicular MoO_3[010] row, which is preferentially epitaxied along a metallic row of the molybdenum facet. During their growth, MoO_3[100] rows become oriented perpendicular to the initial molybdenum surface, while MoO_3(010) planes are built up by periodic arrangement of these MoO_3[100] rows. The periodic stacking of these MoO_3(010) planes never seems to be obtained.

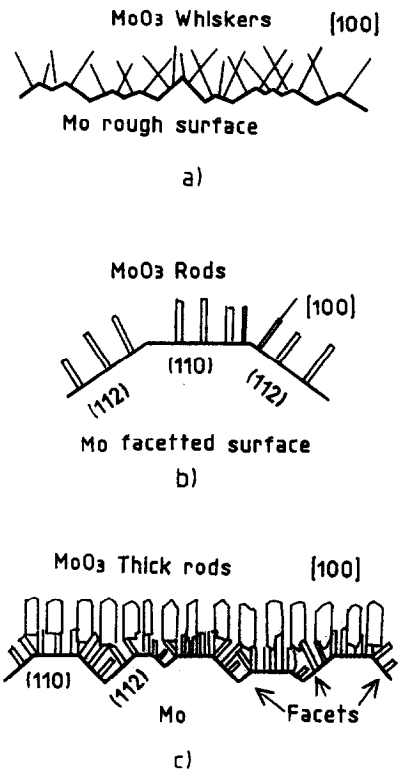

FIG. 8. Schematic pictures of the three main oxidation steps of the Mo(110) surface: (a) formation of perpendicular MoO_3[100] whiskers onto the rough surface, (b) growth of the whiskers normal to the surface facets, (c) far from the metal–oxide interface, growth of thick MoO_3[100] rods, well structured, normal to the Mo(110) surface.

3.1.3. Temperature of 820 K

At 820 K, for a pressure of 2.7×10^3 Pa oxygen, molybdenum oxidizes immediately in volatile MoO_3 as revealed by the blue color of the sample holder. Under 4×10^4 Pa oxygen, MoO_3 sublimation is lower. Auger spectra and RHEED patterns prove the formation of MoO_3 onto the Mo(110) surface at an oxidation stage which corresponds to the last oxidation stage observed at 720 K.

3.1.4. Conclusion

From these results, some important features of the oxidation process emerge. The molybdenum oxides grown by interaction of oxygen at high pressure on a Mo(110) surface are the stoichiometric and stable MoO_2 and MoO_3 oxides. Nonstoichiometric molybdenum oxides and even the more stable Mo_4O_{11} oxide are not evidenced at any stage of the oxidation process.

MoO_2 is generated at the lower temperature which corresponds to carbon adsorption, as flat crystallites expitaxied on the Mo(110) surface and in the same orientation to those observed at low oxygen pressure (1.3×10^{-5} Pa). It constitutes a passive film toward the process of molybdenum oxidation.

MoO_3 is built up by successive structural steps (Fig. 8), from MoO_3[100] rows which order farther from the metal–oxide interface, in the layered structure of orthorhombic MoO_3, with some stacking faults of the MoO_3(010) layers. The MoO_3[100] rows first

grow perpendicular to the metallic facets formed during the oxidation process. Such faceting was previously observed during MoO_2 formation onto the Mo(110) surface (*10*).

The formation of MoO_2 associated with carbon adsorption and of MoO_3 and simultaneous metallic facets on the Mo(110) surface questions whether MoO_3 grows directly from the metal without intermediate formation of MoO_2, whether the MoO_2 formation is induced by the carbon adsorption as a reducing element.

To bring out the oxidation mechanism at the Mo(110) surface at those moderate temperature and high oxygen pressure ranges, oxidation experiments are carried out from a Mo(110) surface covered either partially with MoO_2 crystallites, or with a Mo_2C film.

3.2 Oxidation on the Mo(110) Surface Partially Covered with MoO_2 Crystallites

3.2.1. Characterization of the MoO_2 Crystallites on Mo(110) Surface

MoO_2 is obtained by interaction of oxygen at 2.6×10^{-5} Pa pressure, for a 5-hr exposure, with the Mo(110) surface at 1023 K.

The Auger spectra attest of the formation of a noncovered film of MoO_2 onto the Mo surface (about 40%): the ratios of the peak-to-peak heights Mo(220)/Mo(187) = 0.75 and O(510)/Mo(220) = 1.5 lie between the standard ratios of a Mo surface (0.85 and 0) and a MoO_2 surface (0.61 and 3).

Likewise, RHEED patterns (Fig. 9a) characterize simultaneously the slightly rough Mo(110) surface (modulated streaks) and the MoO_2 crystallites (network of spots) which are in epitaxial relationships:

$$MoO_2(010)_{[100]} \text{ or } _{[001]} \text{ or } _{[101]} \parallel Mo(110)_{[001]}$$

Some stacking faults in the MoO_2[100] or [001] or [101] rows are evidenced by reciprocal planes of diffuse intensity in the diffraction patterns.

Note that, in the monoclinic MoO_2 structure, both the $MoO_2(010)_{[001]}$ and the $MoO_2(010)_{[101]}$ orientations are equivalent. Figure 10 shows one of these epitaxial relations: the close MoO_2[100] row of molybdenum atoms lies parallel to the close Mo[1$\bar{1}$1] row. The parametric misfit of 2.9% expresses the interfacial coherence between the Mo(110) surface and the MoO_2(010) plane, which explains that this epitaxial growth of MoO_2 from the Mo(110) surface is readily obtained.

3.2.2. Oxidation of the "MoO_2–Mo(110)" Surface

The oxidation of the "MoO_2–Mo(110)" surface is realized at 720 K and 2.7×10^3 Pa oxygen pressure.

For a few minutes exposure, the Auger spectra characterize MoO_3 formation and RHEED patterns (Fig. 9b) prove the simultaneous presence of the previous MoO_2 crystallites and the new MoO_3[100] whiskers grown perpendicular to the Mo(110) surface and generated Mo(112) facets.

Compared with the MoO_3[100] whiskers grown from the clean Mo(110) surface during the first exposure:

—the faceting of the Mo(110) surface appeared,

—MoO_3 grew from the Mo(110) surface, irrespective of the MoO_2 crystallites: the epitaxied MoO_2 crystallites do not induce any modification in the structure and the orientation of MoO_3.

Further exposure leads to the fading out of the diffraction spots of MoO_2 crystallites until their disappearance after about 10 hr of exposure (Fig. 9c). The concomitant evolution of the MoO_3 diffraction patterns is interpreted by the progressive change of the perpendicular orientation of the MoO_3[100] whiskers, from the Mo(110) surface and Mo(112) facets to only the Mo(110) surface (Fig. 9d), and by the lateral growth of the MoO_3[100] whiskers in the MoO_3 lamellar structure after a few tens of hours.

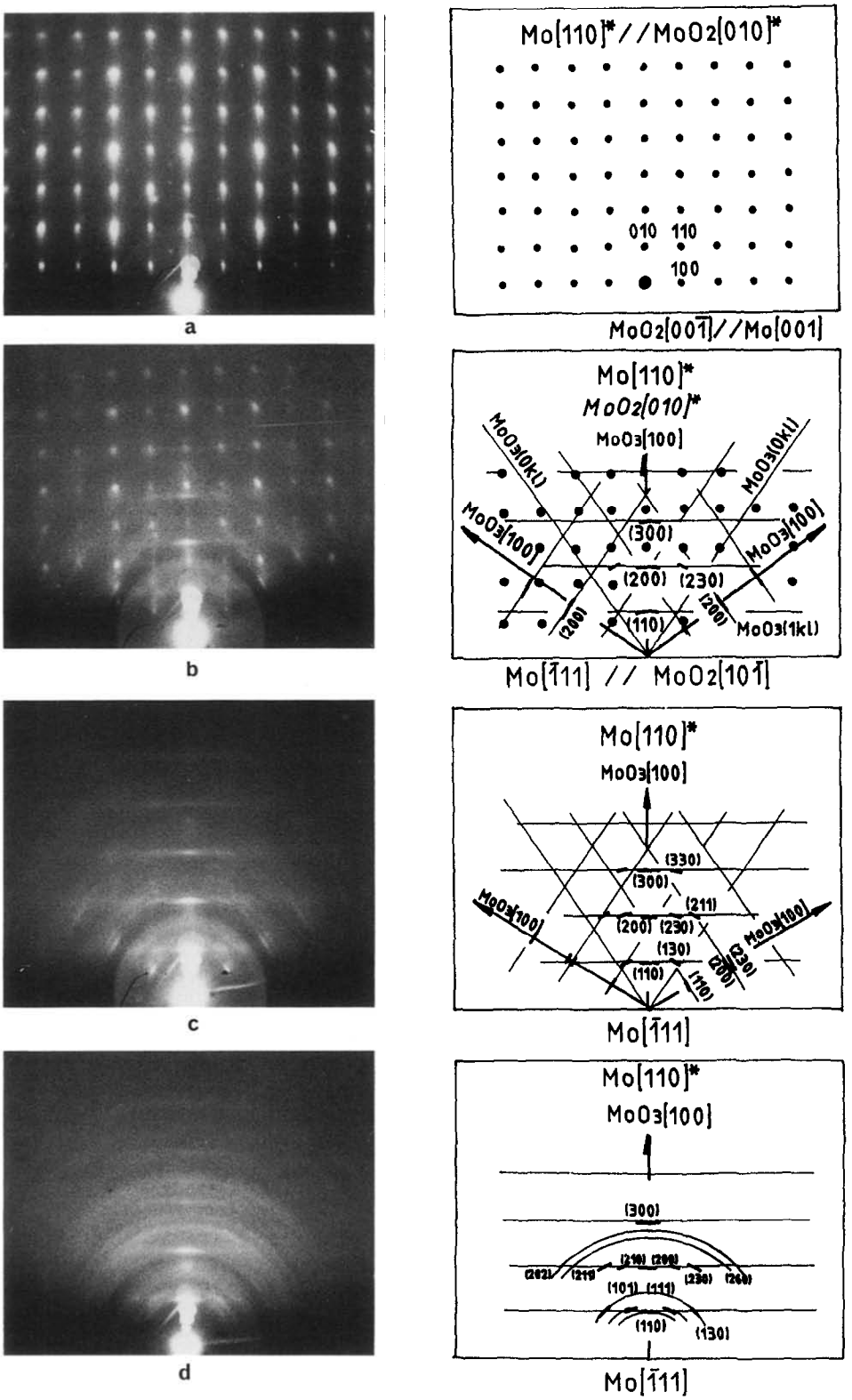

FIG. 9. RHEED patterns from a Mo(110) surface covered partially with MoO_2 crystallites, then oxidized at 720 K and 2.7 × 10^4 Pa oxygen pressure for increasing exposure time: (a) initial surface, (b) after 5 min, (c) after 10 hr (d) after a few tens of hours.

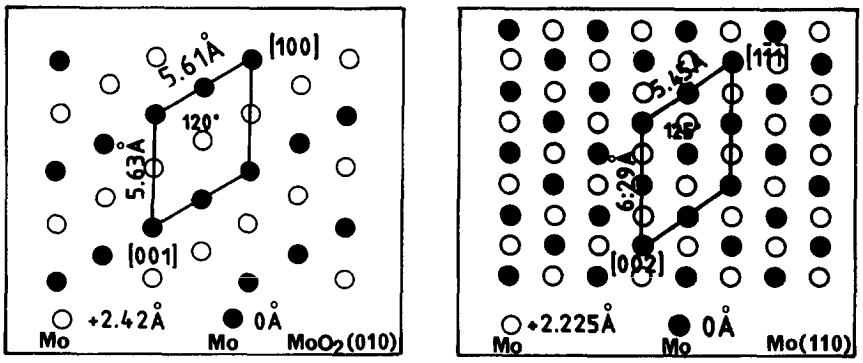

FIG. 10. Positions of molybdenum and oxygen ions in the $MoO_2(010)$ plane with respect to molybdenum atoms in the Mo(110) plane.

These structural features of the MoO_3 growth are similar to those reported previously from the clean Mo(110) surface, only the rate of their evolution seems reduced by the presence of the epitaxied MoO_2 crystallites.

3.2.3. Conclusions

A comparison of the oxidation of a Mo(110) surface and a Mo(110) surface partially covered with MoO_2 crystallites emphasizes the protective nature of the MoO_2 crystallites for further oxidation as soon reported for Mo(110) oxidation at lower temperature (620 K) and supports the oxidation process of the molybdenum leading to the direct formation of MoO_3, without any intermediate formation such as that of MoO_2 or nonstoichiometric molybdenum oxide.

3.3 Oxidation on the Mo(110) Surface Covered with a Mo_2C Film

3.3.1. Characterization of the Mo_2C Film on the Mo(110) Surface

The Mo_2C phase is obtained during the cleaning procedure of the Mo(110) surface, when sputtered by argon ions and annealed at 1200 K under vacuum (see Section 2.2).

Auger spectra (Fig. 1c) reveal the molybdenum carbide formation by the characteristic shape of the carbon KL_2L_2 transition peak (55). The molybdenum $M_{4,5}VV$ and $M_{4,5}N_{2,3}V$ transition peaks have the same shape and energy as those characteristic of a clean Mo surface but their intensity ratio, Mo(220)/Mo(187) = 0.76, is lower. The intensity ratio C(272)/Mo(220) = 0.6.

RHEED patterns (Fig. 11a) consist of a newtork of slighly modulated streaks, normal and oriented in relation with the Mo(110) surface. Quantitative interpretation yields a pseudohexagonal network with a rectangular surface unit cell ($a = 3 \pm 0.05$ Å and $c = 4.66 \pm 0.05$ Å with the ratio $a/c = 0.643$) and an interplanar distance of 2.62 $\pm$ 0.05 Å close to the hexagonal value $a\sqrt{3}/2 = 2.60$ Å. This network is compared with the hexagonal Mo_2C network of a very close unit cell: $a = 3.0124$ Å and $c = 4.7352$ Å with the ratio $a/c = 0.636$) (ASTM 35-587). It is interpreted by the formation of a slightly rough film of Mo_2C in the epitaxial strain onto the Mo(110) surface with the orientation relationships $Mo_2C(100)_{[010]} \parallel Mo(110)_{[001]}$.

Diffuse diffraction lines observed at the $Mo_2C[001]$ azimuth attest to stacking faults of the hexagonal $Mo_2C(001)$ planes which are perpendicular to the Mo(110) surface along the Mo[001] directions.

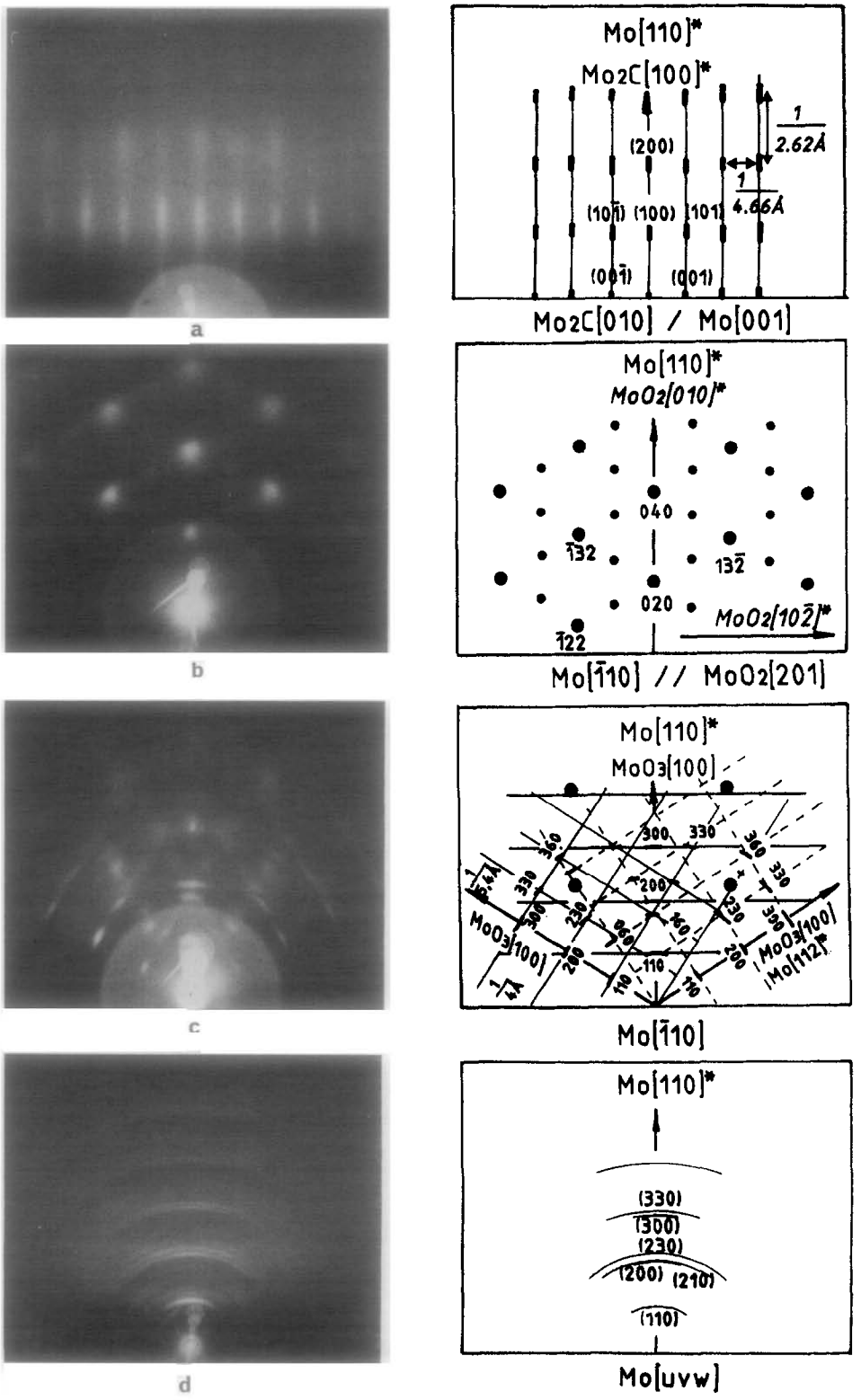

FIG. 11. RHEED patterns from a Mo(110) surface covered with Mo_2C film, then oxidized at 720 K and 2.7×10^4 Pa oxygen pressure for increasing exposure time: (a) initial surface, (b) after a half hour, (c) after 7 hr (d) after several hours.

3.3.2. Oxidation of the "$Mo_2C(100)$–$Mo(110)$" Surface

The oxidation of the Mo(110) surface covered with the epitaxied $Mo_2C(100)$ film is realized in the same conditions at 720 K and 2.7×10^3 Pa oxygen pressure.

After a half hour exposure, RHEED patterns (Fig. 11b) attest to the disappearance of $Mo_2C(100)$ film (no streaks are visible) and the presence of MoO_2 crystallites (network of rather large and diffuse spots).

The MoO_2 crystallites are oriented in relation with the $Mo_2C(100)$ film and precisely in the same epitaxial relations as related previously for MoO_2 crystallites from clean Mo(110) under 10^{-5} Pa oxygen pressure:

$$MoO_2(010)_{[100]} \text{ or } {}_{[001]} \text{ or } {}_{[101]} \parallel Mo_2C(100)_{[010]} \parallel Mo(110)_{[001]}.$$

Note that the larger and more diffuse diffraction spots reveal a very small size or structural defects of these MoO_2 crystallites. Auger spectra confirm the formation of MoO_2 and both intensity drop and shape change of the carbon KL_2L_2 transition peak prove the carbon removal by oxidation.

For 7-hr exposure (Fig. 11c), while the MoO_2 crystallites are still present on the surface, MoO_3 becomes visible in the form of $MoO_3[100]$ whiskers perpendiculary oriented in relation to the Mo(110) surface and Mo(112) facets.

At this oxidation step, the structural features are roughly similar to those reported for the Mo(110) surface partially covered with MoO_2 crystallites. Yet detailed analysis of the RHEED patterns gives more structural information on the growth mode of MoO_3:

on the Mo(110) surface, the $MoO_3[100]$ whiskers have the preferential orientation

$$MoO_3(100)_{[010]} \parallel Mo(110)_{[1\bar{1}1]},$$

on the Mo(112) and Mo(11$\bar{2}$) facets, the observed epitaxial relation

$$MoO_3(100)_{[010]} \parallel Mo(112)_{[11\bar{1}]}$$

is associated with an ordered stacking of the $MoO_3[100]$ rows (5.4 Å periodicity) along the Mo[11$\bar{1}$] direction (5.45 Å parameter).

After several hours exposure (Fig. 11d), there are no more MoO_2 crystallites and the growth of $MoO_3[100]$ whiskers goes on, as described at the first oxidation step from the clean Mo(110) surface.

3.3.3. Conclusion

For oxidation at moderate temperature and high oxygen pressure, it appears that the formation of MoO_2 is always associated with carbon. The oxidation of the clean Mo(110) surface leads only to the formation of MoO_3.

The comparative analysis underlines the fundamental differences between the formation mechanism of the MoO_2 and MoO_3 oxides. These differences seem inherent in the nature of both oxides and are expressed structurally as well as by their specific physicochemical properties.

MoO_2 grows in the form of epitaxied crystallites with few structural defects. The MoO_2 crystallites are generated until the formation of a covered film which stops the oxidation process of the molybdenum.

MoO_3 builds up by progressive structural steps, perpendicular to the Mo(110) surface and the principal Mo(112) facets with little interfacial relationship. Its formation induces the faceting of the molybdenum surface.

3.4. Oxidation of the Mo(100) Surface

The oxidation of the Mo(100) surface is realized at 2.7×10^3 Pa oxygen pressure and at both 620 and 720 K.

3.4.1. Temperature of 620 K

For the first minutes of exposure, modifications in the Auger spectra characterize the MoO_3 formation and the outside carbon adsorption in the graphite form. At the same time, RHEED patterns of the smooth

Mo(100) surface (Fig. 12a) fade into a diffuse intensity background.

After another exposure, no noticeable changes occur either in the Auger spectra or in the RHEED patterns.

These results prove the formation of MoO_3 nuclei, of amorphous structure or of nanometric size. At the 620 K temperature, the oxidation reaction does not progress more over this oxidation stage.

3.4.2. Temperature of 720 K

For the first exposure and further exposures the AES analysis attests to the immediate and lasting formation of MoO_3 as observed from the Mo(110) surface.

Arising from the first few minutes exposure, the first modification of the RHEED patterns consists of the fading of diffraction streaks of the initial Mo(100) surface into a diffuse intensity background.

After about 2 hr exposure, two new superimposed diffraction patterns become apparent (Fig. 12b):

(1) The set of $MoO_3(hk0)$ arcs ordered into lines with $MoO_3[100]$ periodicity (4 Å) and parallel to the Mo(100) surface. It characterizes the presence of the $MoO_3[100]$ whiskers perpendicular to the Mo(100) surface.

(2) A double network of streaks, perpendicular and oriented in relation to the Mo(100) surface. These diffraction features are due to $MoO_3(010)$ plates parallel to the Mo(100) surface and oriented in the two equivalent relations

$$MoO_3(010)_{[001]} \parallel Mo(100)_{[011] \text{ and } [0\bar{1}1]}.$$

For 10 hr exposure, a new modification in the RHEED patterns (Fig. 12c) arises: the set of $MoO_3(hk0)$ arcs disappears, while the double network of streaks characteristic of the $MoO_3(010)$ plates fades. A new set of large $MoO_3(h0l)$ and $MoO_3(h1l)$ arcs ordered into parallel lines with the $MoO_3[100]$ periodicity (4 Å) is visible at any azimuth. At both the Mo[011] and the Mo[$0\bar{1}1$] azimuth, these MoO_3 arcs intersect precisely the $MoO_3(010)$ streaks, which are $MoO_3[001]$ spaced. These new diffraction features characterize perpendicular $MoO_3(010)$ plates, whose $MoO_3[100]$ axes are at $\pm 10°$ around the normal of the Mo(100) surface.

After several tens of hours exposure, RHEED patterns (Fig. 12d) consist of the whole disappearance of the $MoO_3(010)$ streaks and the presence of a set of $MoO_3(hkl)$ rings, with intensity modulations. The intensity maxima of the previous $MoO_3(h0l)$ and $MoO_3(h1l)$ rings are still visible.

This last evolution is interpreted by the growth in thickness of the $MoO_3(010)$ plates which are oriented perpendicular to the Mo(100) surface in the relations

$$MoO_3(010) \perp Mo(100)$$

$$MoO_3[100] \text{ at } \pm 10° \text{ Mo}[100].$$

3.4.3. Conclusion

The initial oxidation stage of the Mo(100) surface corresponds to the formation of MoO_3 nuclei of amorphous structure or nanometric size. It is the only stage observed at 620 K, corresponding to the check of the oxidation reaction.

At 720 K, the molybdenum oxidation progresses only to the formation of the orthorhombic MoO_3, excluding the MoO_2 or the nonstoichiometric molybdenum oxides (Fig. 13).

The properties of the metal–oxide interface, between the Mo(100) surface and the $MoO_3(010)$ layer, induce:

—the formation of $MoO_3(010)$ plates epitaxied onto the Mo(100) surface,

—the stability of the metallic Mo(100) surface: no surface faceting arises during the oxidation reaction, while Mo(100) faceting is reported by several authors at ambient temperature and low oxygen pressure (*3, 9*).

The oxidation mechanism favors the formation of MoO_3 crystals whose $MoO_3(010)$

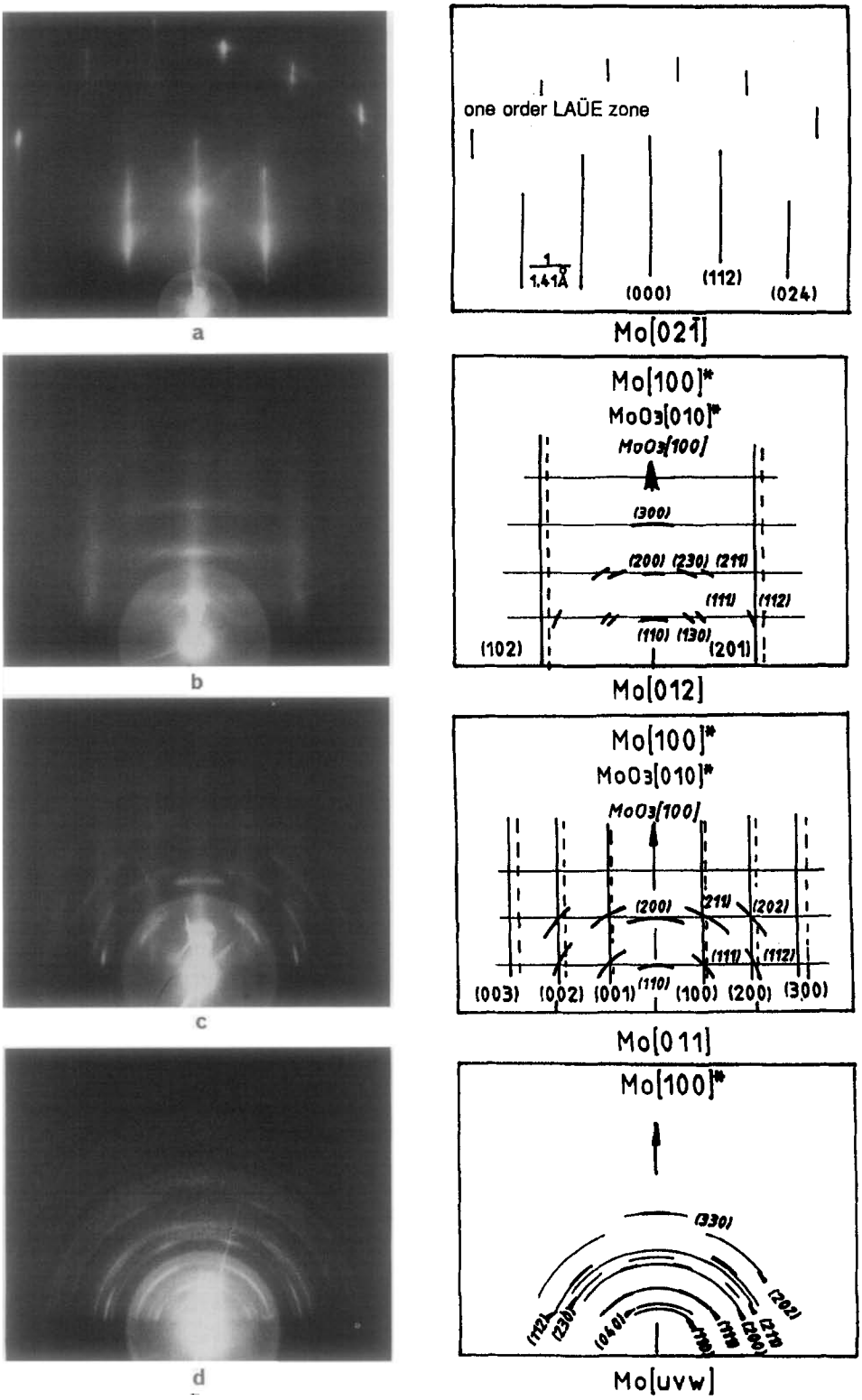

FIG. 12. RHEED patterns from a Mo(100) surface oxidized at 720 K and 2.7×10^4 Pa oxygen pressure for increasing exposure time: (a) initial Mo(100) surface, (b) after 2 hr, (c) after 10 hr (d) after several tens of hours.

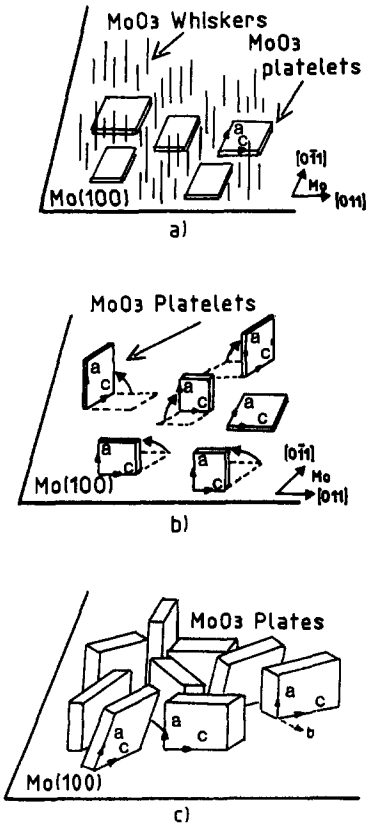

FIG. 13. Schematic pictures of the three main oxidation steps of the Mo(100) surface: (a) formation of perpendicular MoO_3[100] whiskers and epitaxied MoO_3(010) platelets onto the smooth Mo(100) surface, (b) orthogonal orientation of the MoO_3(010) platelets, (c) growth of thick MoO_3(010) plates normal to the Mo(100) surface.

layers and MoO_3[100] rows grow perpendicular to the molybdenum surface.

This preferential growth gives rise to the tilting at about 90° of the MoO_3(010) plates initially epitaxied onto the surface.

3.5 Oxidation on the Mo(111) Surface

The oxidation on the Mo(111) surface is realized at 2.7×10^3 Pa oxygen pressure and at the one 720 K temperature.

3.5.1. Initial Mo(111) Surface

The Mo(111) surface, known as an instable surface (*16, 19*), is obtained slightly rough, with little oxygen chemisorption.

The Mo(111) surface produces Auger spectra, characteristic of a molybdenum surface, identical to those obtained from the Mo(110) and Mo(100) surfaces. The oxygen chemisorption, less than one monolayer, is evidenced by the oxygen peak O(550) of relative peak-to-peak height O(550)/Mo(220) = 0.2.

The RHEED patterns, reproduced in Fig. 14a, attest to a slightly rough surface by the slight intensity modulation of the diffraction streaks and oxygen chemisorption by the presence of diffuse diffraction lines which form Mo($1\bar{1}0$)*, Mo($\bar{1}01$)*, and Mo($01\bar{1}$)* diffuse planes. The oxygen chemisorption produces defects in the arrangement of the three equivalent Mo[$1\bar{1}0$], Mo[$\bar{1}01$], and Mo[$01\bar{1}$] rows of the Mo(111) surface.

3.5.2. Oxidation at 720 K

Since the first exposure, Auger spectra attest to the formation of MoO_3 as observed from the Mo(110) and Mo(100) surfaces.

The RHEED patterns prove the formation of oxide nuclei of amorphous structure or of nanometric size by the fading of Mo(111) diffraction streaks into a diffuse intensity background.

This oxidized state of the surface changes after about 3 hr exposure, as characterized by the RHEED patterns. A set of MoO_3(*hkl*) rings appears with less or more diffuse intensity. Intensified arcs order into two networks of lines with the MoO_3[100] periodicity (4 Å). At the three equivalent azimuths, Mo[$1\bar{1}0$], Mo[$01\bar{1}$], and Mo[$\bar{1}01$] (Figs. 14b, and 14d), the two networks of lines are tilted respectively at 35° and 20° to the Mo(111) surface, which is parallel to the Mo(110) and Mo(112) facets and their equivalent facets. At the intermediate azimuths Mo[$\bar{2}11$], Mo[$1\bar{2}1$], and Mo[$11\bar{2}$] (Fig. 14c), they are symmetric and tilted at 35° to the Mo(111) surface, which is parallel to the Mo(110), Mo(011), and Mo(101) equivalent facets.

These diffraction features are comparable to the previous ones observed from the Mo(110) surface. They are interpreted by

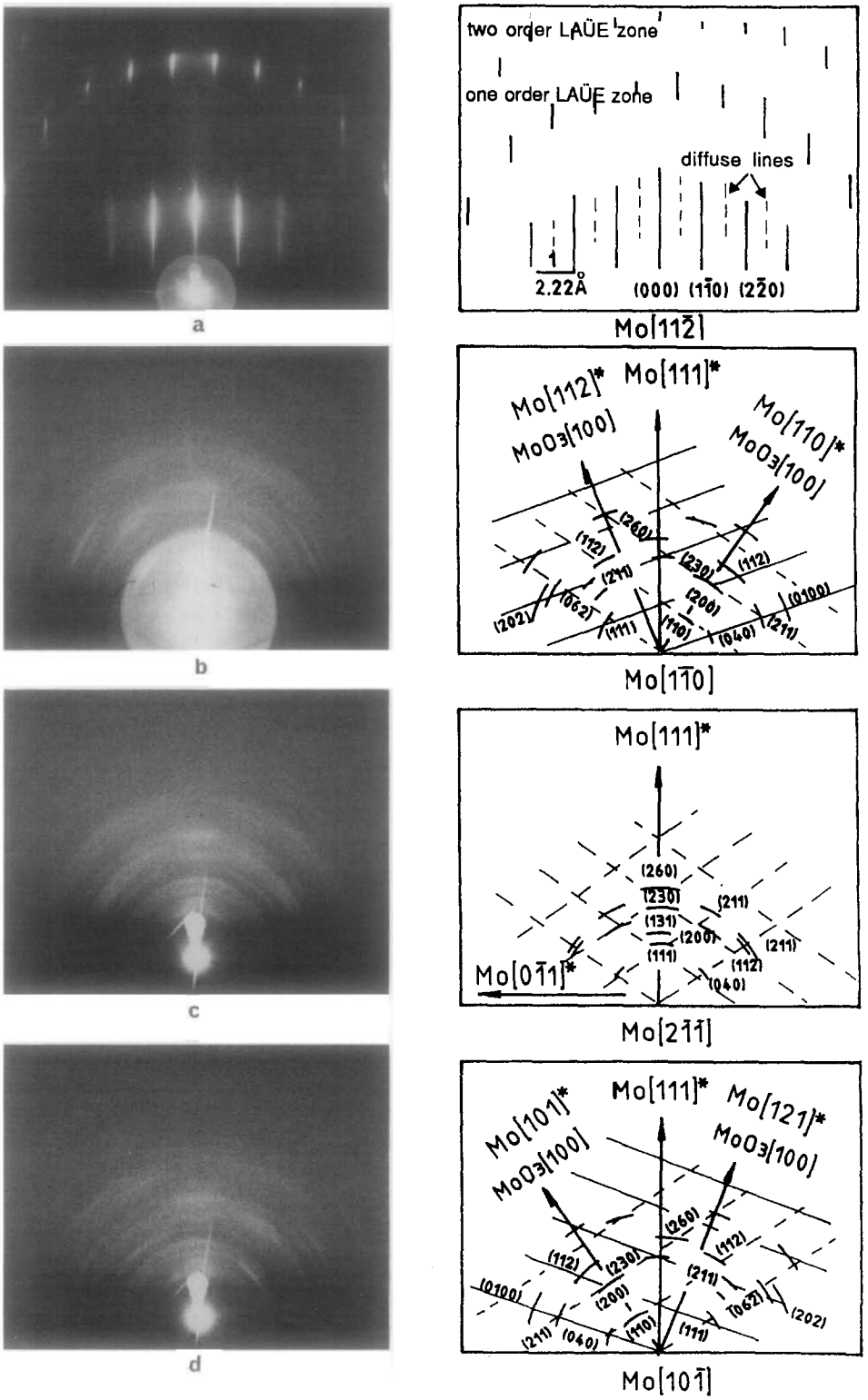

FIG. 14. RHEED patterns from a Mo(111) surface oxidized at 720 K and 2.7 × 10^4 Pa oxygen pressure for increasing exposure time: (a) initial Mo(111) surface, (b), (c), (d) after 3 hr along various azimuths.

the formation of crystalline MoO_3[100] rods growing perpendicular to the main Mo(110), Mo(011), and Mo(101) facets and the Mo(211), Mo(121), and Mo(112) facets produced on the Mo(111) surface.

No evolution of this oxidized state of the molybdenum surface appears, even after several hours exposure.

3.5.3. Conclusion

The interaction of oxygen with a Mo(111) surface leads simultaneously to the faceting of the initial surface onto the more stable Mo(110) and Mo(112) planes and to the direct formation of crystalline MoO_3[100] rods perpendicular to each metallic facet, which is with the orientation observed on a Mo(110) surface.

The formation of one molybdenum oxide, other than MoO_3 trioxide, is not observed. The presence of an epitaxied oxide film, such as MoO_3(010) plates formed onto Mo(100) surface, is also not observed.

The immediate faceting of the Mo(111) surface associated with the MoO_3 crystallite formation is related to the unstable nature of the Mo(111) plane compared to that of the Mo(110) plane and to the nonformation of an epitaxied oxide film at the first oxidation stage, as onto the Mo(100) plane.

3.6. Discussion—Conclusion

From the main results reported in Table II, fundamental points should be emphasized:

3.6.1 Stability of the Metallic Surfaces and MoO_3 Formation

In the experimental conditions of MoO_3[100] whisker formation (620–820 K and 2.7×10^4 Pa oxygen pressure), the Mo(110) and Mo(111) surfaces are faceted in the Mo(100), Mo(110), and Mo(112) planes. Such faceting is also observed in the (T, P_{O2}) conditions of oxygen chemisorption and MoO_2 formation, at higher temperatures (800–1050 K) and lower oxygen pressures (5×10^{-6} Pa to 10^{-4} Pa) (*10, 12, 16, 19*). Between the two mechanisms of faceting generally proposed (*4, 7*), the facets seem rather generated by sublimation of atoms in the molybdenum oxide form along preferential crystallographic directions: indeed, in such a (T, P_{O2}) domain where MoO_3 is formed, the mobility of $(MoO_3)_{3n}$ species is important (*42, 43*). Moreover this $(MoO_3)_{3n}$ hypermobility seems related to the fact that MoO_3 is generated as MoO_3[100] whiskers instead of well-structured MoO_3 crystallites.

3.6.2 Chemical State of the Metallic Surface and Steps of MoO_3 Formation

The MoO_2 formation as an intermediate step of MoO_3 formation has been previously reported from thermogravimetric studies on the oxidation of polycrystalline molybdenum foils by interaction of oxygen at about 10^4 to 10^5 Pa pressure at the 673–998 K temperature range (*27*).

The results seem to prove that MoO_3 is formed directly by interaction of oxygen with molybdenum. MoO_2 is growing either from oxidation of a Mo_2C film or when there is carbon adsorption at lower temperature. In any case, the formation of MoO_2 crystallites is not an intermediate step of the MoO_3 formation; moreover, its presence on molybdenum impedes the oxidation of molybdenum into MoO_3.

3.6.3 Crystalline Orientation of the Molybdenum Surface, Oriented MoO_3 Nucleation and Growth

(*a*) *Structural relations within the metal–oxide interface: epitaxial factor in the oxide nucleation.* The structural features of the first MoO_3 nuclei which depend on the crystalline orientation of the molybdenum surface (see Sections 3.1.2, 3.4.2, 3.5.2), express the specific properties of the metal–oxide interface.

TABLE II

MAIN STRUCTURAL STEPS OF MOLYBDENUM OXIDE GROWN BY OXYGEN INTERACTION ONTO THE THREE MOLYBDENUM SURFACES (P_{O_2} = 2.7 × 10^3 Pa AND T = 720 K) IN FUNCTION OF EXPOSURE TIMES

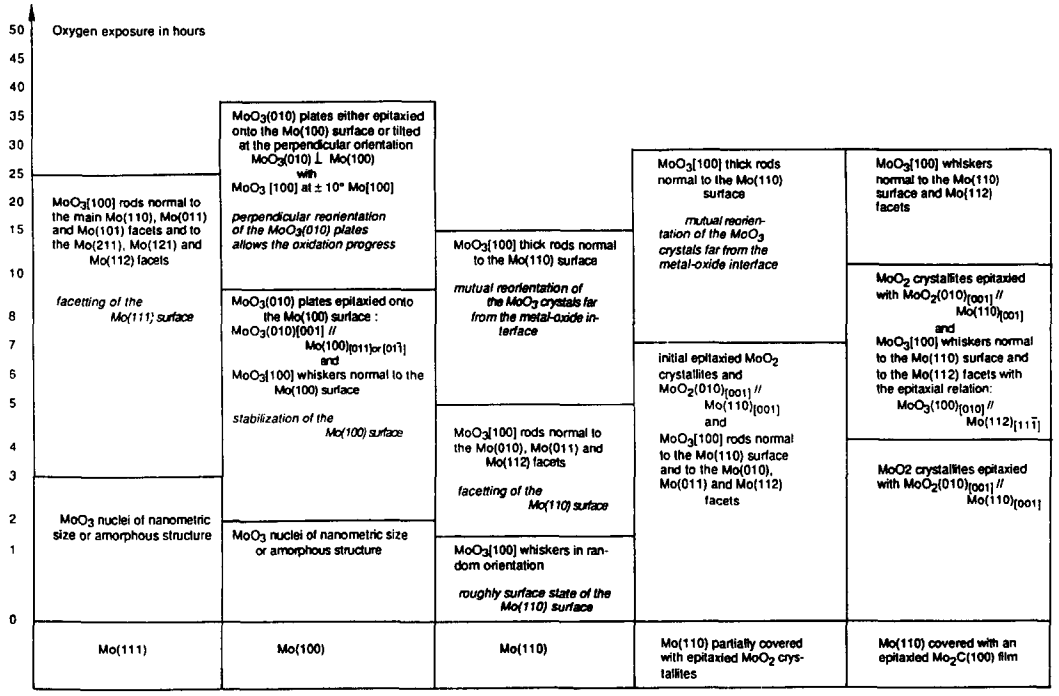

The Mo(100) surface produces oriented MoO_3(010) plates, inducing its stabilization. In this case only, there is a 2D interfacial relation between the metallic and the oxide surface. Figure 15 represents both interfacial planes by the relative atomic positions of molybdenum and oxygen. It evidences that:

(1) the closest molybdenum rows in MoO_3, the zig-zag MoO_3[001] rows, are along the Mo[011] rows, that is along the zig-zag Mo1/2[111]–Mo1/2[$\bar{1}$11] close rows in the molybdenum.

(2) the pseudosquare subnetwork of oxygen of MoO_6 octahedra (2.71 Å side) is along the square network of molybdenum (3.147 Å side).

The epitaxy relationships between the oxygen network and molybdenum close row could explain the formation of MoO_3(010) plates oriented onto the Mo(100) surface as

$$MoO_3(010)_{[001]} \parallel Mo(100)_{[011]} \text{ or } _{[0\bar{1}1]}.$$

The Mo(110) and Mo(111) surfaces generate MoO_3[100] whiskers normal to the facets simultaneously produced. A short range order of the MoO_3[100] rows is always observed in the MoO_3[010] direction lying on the metallic surface.

Marked preferential orientation of the MoO_3[010] rows of these MoO_3[100] whiskers onto Mo(110) and Mo(111) surfaces is not well observed, except for the Mo(112) facets, where the epitaxial relation MoO_3[010] ∥ Mo[11$\bar{1}$] is well evidenced. Moreover, in this case, the initial MoO_3[010] periodicity fits the Mo[11$\bar{1}$] one, which could be explained by the nature of the

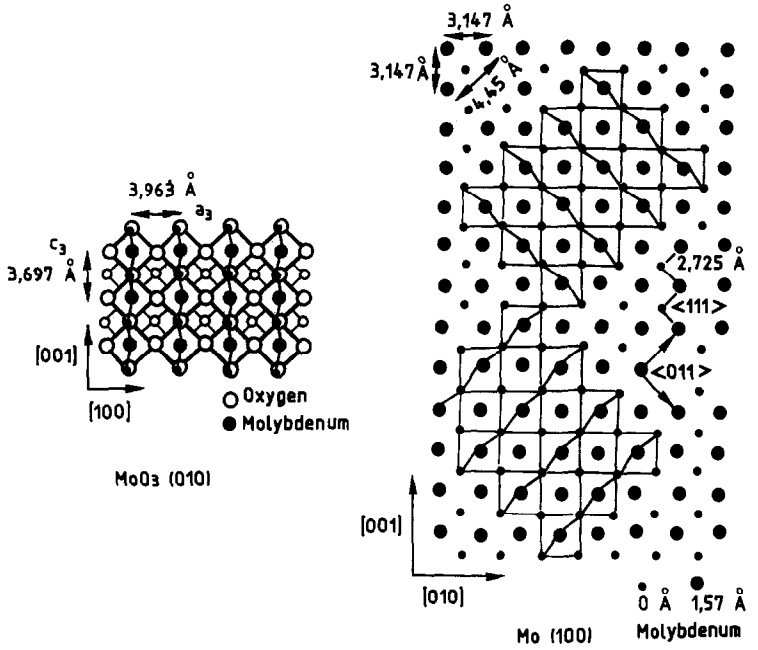

FIG. 15. Positions of molybdenum and oxygen ions in $MoO_3(010)$ plane with respect to molybdenum atoms in Mo(100) plane.

bonds in these $MoO_3[010]$ directions, which are Van der Waals interactions (see Fig. 2).

From the same structural considerations, it could be explained that the lamellar $MoO_3(010)$ plane is not initially built. Indead the close $MoO_3[001]$ rows, the zig-zag rows in the $MoO_3(010)$ planes, do not fit any Mo row in the interfacial molybdenum planes (8.5% mismatch for the best parametric agreement) (Fig. 16).

(*b*) *Structural relations between the oxide nucleation and its growth: dynamic factors of the reaction.* During their growth, from any parent metallic surface, the oxide nuclei build up in the orthorhombic MoO_3 structure and orientate their lamellar $MoO_3(010)$ planes perpendicular to the metallic surface and their close $MoO_3[001]$ rows onto close Mo rows of the metallic surface. The results obtained from the Mo(100) surface underline these growth factors, because of an orthogonal reorientation of the initial $MoO_3(010)$ plates epitaxied onto the Mo(100) surface.

These structural features of the nucleation and growth, and their relationships, allow the dissociation of factors related to the metal–oxide interfacial relations to factors of the dynamic of the oxidation reaction:

—the interfacial forces induce the non-well-structured oxide nuclei, as $MoO_3[100]$ rows normal to the metallic surface. Some order of the $MoO_3[100]$ rows along $MoO_3[010]$ direction could be explained by structural relationships in the metal–oxide interface.

—the preferential diffusion of oxygen along the lamellar $MoO_3(010)$ planes through the orthorhombic MoO_3 structure induces their orientation normal to the reaction plane.

Such interpretation of nucleation and growth mechanisms of MoO_3 produced by

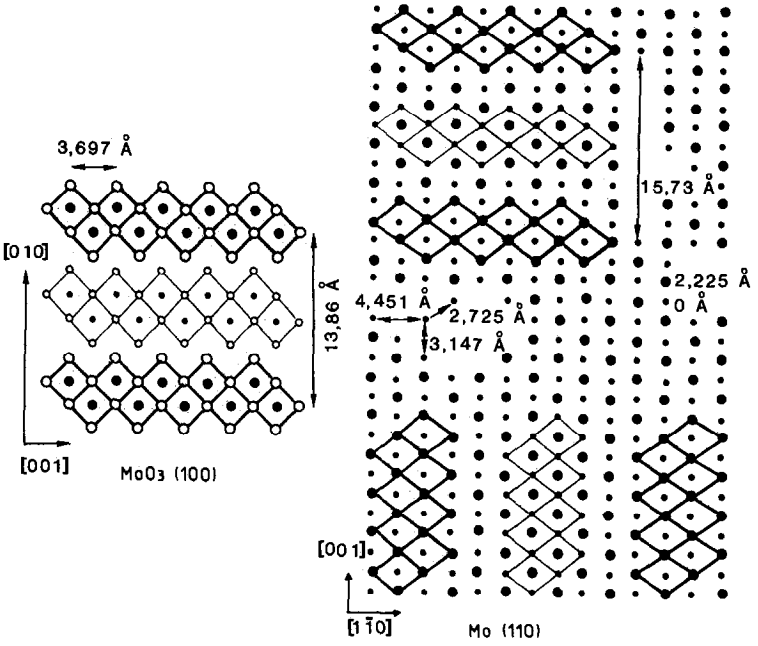

FIG. 16. Positions of molybdenum and oxygen ions in MoO_3(100) plane with respect to molybdenum atoms in Mo(110) plane.

the interaction of oxygen with a molybdenum surface explains previous (*35*) and further (*36*) results of the morphological and structural study of the MoO_3 layer generated from polycrystalline molybdenum foils.

References

1. T. W. HAAS AND A. G. JACKSON, *J. Chem. Phys.*, **44**(8), 2921 (1966).
2. J. FERRANTE AND G. BARTON, NASA Technical Note TN D-4735, p. 1449 (1968).
3. K. HAYEK, H. E. FARNSWORTH, AND R. L. PARK, *Surface Sci.* **10,** 429 (1968).
4. J. C. TRACY AND J. M. BLAKELY, *Surface Sci.* **13,** 313 (1969).
5. H. K. A. KAN AND S. FEUERSTEIN, *J. Chem. Phys.* **50**(8), 3618 (1969).
6. G. J. DOOLEY III AND T. W. HAAS, *J. Chem. Phys.* **52,** 461 (1970); *J. Vacuum Sci. Technol* **7,** 1570 (1970).
7. A. E. LEE AND K. E. SINGER, *Proc. R. Soc. London A* **323,** 523 (1971).
8. D. TABOR AND J. M. WILSON, *J. Crystal Growth* **9,** 60 (1971).
9. H. M. KENNETT, A. E. LEE, AND J. M. WILSON, *Proc. R. Soc. London A* **331,** 429 (1972).
10. J. BRÜCKNER, *Krist. Tech.* **9**(6), 647 (1974).
11. R. RIWAN, C. GUILLOT, AND J. PAIGNE, *Surface Sci.*, **47,** 183 (1975).
12. H. M. KENNETT AND A. E. LEE, *Surface Sci.* **48,** 591 (1975).
13. E. BAUER AND H. POPPA, *Surface Sci.* **88,** 31 (1979).
14. E. I. KO AND R. J. MADIX, *Surface Sci.* **109,** 221 (1981).
15. E. BAUER AND H. POPPA, *Surface Sci.* **127,** 243 (1983).
16. C. ZHANG, M. A. VAN HOVE, AND G. A. SOMORJAI, *Surface Sci.* **149,** 326 (1985).
17. J. L. GRANT, T. B. FRYBERGER, AND P. C. STAIR, *Surface Sci.* **159,** 333 (1985).
18. TS. S. MARINOVA, P. K. STEFANOV, AND N. NESHEV, *Surface Sci.* **164,** 196 (1985).
19. C. ZHANG, A. J. GELLMAN, M. H. FARIAS, AND G. A. SOMORJAI, *Mater. Res. Bull.* **20,** 1129 (1985).
20. J. L. GRANT, T. B. FRYBERGER, AND P. C. STAIR, *Appl. Surf. Sci.* **26,** 472 (1986).
21. E. MINNI AND F. WERFEL, *Surf. Interface Anal.* **12,** 385 (1988).

22. P. K. Stefanov and Ts. S. Marinova, *Surface Sci.* **200,** 26 (1988).
23. E. A. Gulbransen and W. S. Wysong, *Met. Technol.* **14,** 2226 (1947).
24. J. W. Hickman and E. A. Gulbransen, *Met. Technol.* **14,** 2144 (1947).
25. B. Lustman, *Met. Prog.* **57,** 629 (1950).
26. R. C. Peterson and W. M. Jr. Fassel, Techn. Report VI Army Ordnance. Contract DA.04.495, ORD 237 (1954).
27. M. Simnad and A. Spilners, *Trans. AIME* **203,** 1011 (1955).
28. M. Gleiser, W. L. Larsen, R. Speiser, and J. W. Spretnak, ASTM Special Publication 171, p. 65 (1955).
29. E. S. Jones, J. F. Mosher, R. Speiser, and J. W. Spretnak, *Corrosion* **14,** 20 (1958).
30. R. W. Bartlett and D. M. Williams, *Trans. Met. Soc. AIME* **212,** 280 (1958).
31. E. A. Gulbransen, K. F. Andrew, and F. A. Brassart, *J. Electrochem. Soc.* **110**(9), 952 (1963).
32. E. A. Gulbransen *Corrosion-Nace* **26**(1), 19 (1970).
33. V. Ya. Kolot, V. I. Tatus, V. F. Rybalko, Ya. M. Fogel, V. V. Vodolazhchenko, and V. M. Evseev, *Soviet Physics-Solid State* **13**(6), 1275 (1972).
34. G. M. Raynaud, *J. Mater. Sci. Lett.* **3,** 965 (1984).
35. B. Mingot, N. Floquet, O. Bertrand, M. Treilleux, J. J. Heizmann, J. Massardier, and M. Abon, *J. Catal.* **118,** 424 (1989).
36. N. Floquet and O. Bertrand, Oxidation of Metals, to be published.
37. T. N. Nowicki and B. M. Birondi, J. de Physique, Proc. Conf. Lake Placid (ISE87) (1987).
38. B. A. Stasliewicz, J. R. Trucker, P. E. Snyder, *J. Am. Chem. Soc.* **78,** 1553 (1956).
39. O. Kubaschewski, E. L. Evans, and C. B. Alcok, "Metalliorgical Thermochemistry," pp. 182–195, Pergamon Press, London (1958).
40. L. Kihlborg, *Ark. Kemi* **21,** 473 (1963).
41. L. L. Y. Chang, B. Phillips, *J. Am. Ceram. Soc.* **52**(10) (1969).
42. J. Berkowitz, M. G. Inghram, and W. A. Chupka, *J. Chem. Phys.* **26**(4), 842 (1957).
43. Y. Ikeda, M. Ito, I. Mizuno, K. Amioka, and G. Matsumoto, *High Temp. Sci.* **16,** 1 (1983).
44. O. Bertrand, N. Floquet, and D. Jacquot, *J. Crystal Growth* **96,** 708 (1989).
45. O. Bertrand, P. Dufour, N. Floquet, and L. C. Dufour, *Phys. Status Solidi.* (a) **71,** 511 (1982).
46. L. C. Dufour, O. Bertrand, and N. Floquet, *Surface Sci.* **147,** 396 (1984).
47. O. Bertrand, N. Floquet, and D. Jacquot, *Surface Sci.* **164,** 305 (1985).
48. L. Kihlborg, *Ark. Kemi* **21,** 357 (1963).
49. A. Magneli, *Ark. Kemi Mineral. Geol. A* **24** 2 (1946).
50. B. G. Brandt and A. C. Skapski, *Acta. Chem. Scand* **21,** 661 (1967).
51. A. Magneli, *Acta. Crystallogr.* **6,** 495 (1953).
52. L. Kihlborg, *Arkiv. Kemi.* **21,** 471 (1963).
53. T. T. Lin and D. Lichtman, *J. Vacuum Sci. Technol.* **15**(5), 1689 (1978).
54. S. Yashonath, P. Sen, M. S. Hedge, and C. N. Ramachandra Rao, *J. Chem. Soc. Faraday Trans. 1* **79,** 1229 (1983).
55. T. W. Haas and J. T. Grant, *Phys. Lett. A* **30,** 272 (1969).